JOURNAL OF GEOPHYSICAL RESEARCH, VOL. 111, D15308, doi:10.1029/2005JD006680, 2006

Evaluation of space-based constraints on global nitrogen oxide emissions with regional aircraft measurements over and downwind of eastern North America

Randall V. Martin,[1,2] Christopher E. Sioris,[3] Kelly Chance,[3] Thomas B. Ryerson,[4] Timothy H. Bertram,[5] Paul J. Wooldridge,[5] Ronald C. Cohen,[5] J. Andy Neuman,[6,7] Aaron Swanson,[6,8,9] and Frank M. Flocke[10]

Received 17 September 2005; revised 20 April 2006; accepted 1 May 2006; published 11 August 2006.

[1] We retrieve tropospheric nitrogen dioxide (NO_2) columns for May 2004 to April 2005 from the SCIAMACHY satellite instrument to derive top-down emissions of nitrogen oxides ($NO_x = NO + NO_2$) via inverse modeling with a global chemical transport model (GEOS-Chem). Simulated NO_2 vertical profiles used in the retrieval are evaluated with airborne measurements over and downwind of North America (ICARTT); a northern midlatitude lightning source of 1.6 Tg N yr^{-1} minimizes bias in the retrieval. Retrieved NO_2 columns are validated ($r^2 = 0.60$, slope = 0.82) with coincident airborne in situ measurements. The top-down emissions are combined with a priori information from a bottom-up emission inventory with error weighting to achieve an improved a posteriori estimate of the global distribution of surface NO_x emissions. Our a posteriori NO_x emission inventory for land surface NO_x emissions (46.1 Tg N yr^{-1}) is 22% larger than the GEIA-based a priori bottom-up inventory for 1998, a difference that reflects rising anthropogenic emissions, especially from East Asia. A posteriori NO_x emissions for East Asia (9.8 Tg N yr^{-1}) exceed those from other continents. The a posteriori inventory improves the GEOS-Chem simulation of NO_x, peroxyacetylnitrate, and nitric acid with respect to airborne in situ measurements over and downwind of New York City. The a posteriori is 7% larger than the EDGAR 3.2FT2000 global inventory, 3% larger than the NEI99 inventory for the United States, and 68% larger than a regional inventory for 2000 for eastern Asia. SCIAMACHY NO_2 columns over the North Atlantic show a weak plume from lightning NO_x.

Citation: Martin, R. V., C. E. Sioris, K. Chance, T. B. Ryerson, T. H. Bertram, P. J. Wooldridge, R. C. Cohen, J. A. Neuman, A. Swanson, and F. M. Flocke (2006), Evaluation of space-based constraints on global nitrogen oxide emissions with regional aircraft measurements over and downwind of eastern North America, *J. Geophys. Res.*, *111*, D15308, doi:10.1029/2005JD006680.

1. Introduction

[2] Nitrogen oxide radicals ($NO_x \equiv NO + NO_2$) largely control tropospheric ozone production [*Kasibhatla et al.*, 1991; *Penner et al.*, 1991; *Murphy et al.*, 1993; *Jacob et al.*, 1996], oxidize in the atmosphere to form nitric acid (HNO_3) that affects cloud properties [*Nenes et al.*, 2002] and contributes to aerosol formation [*Adams et al.*, 2001], and subsequently deposit to the surface with implications for marine [*Michaels et al.*, 1996] and terrestrial [*Holland and Lamarque*, 1997] ecosystems. Anthropogenic activity has increased global NO_x emissions by a factor of 3–6 since preindustrial times [*Prather et al.*, 2001]. Assessments of the implications of NO_x emissions usually are based on "bottom-up" inventories as determined by aggregating information about sources from diverse sources such as fuel and land use statistics, in-tunnel measurements of NO_x emission ratios, agricultural data, and estimates of burned areas. "Top-down" information from space-based observa-

[1]Department of Physics and Atmospheric Science, Dalhousie University, Halifax, Nova Scotia, Canada.
[2]Also at Harvard-Smithsonian Center for Astrophysics, Cambridge, Massachusetts, USA.
[3]Harvard-Smithsonian Center for Astrophysics, Cambridge, Massachusetts, USA.
[4]Chemical Sciences Division, Earth System Research Laboratory, NOAA, Boulder, Colorado, USA.
[5]Department of Chemistry, University of California, Berkeley, Berkeley, California, USA.
[6]Cooperative Institute for Research in Atmospheric Sciences, Boulder, Colorado, USA.
[7]Also at Chemical Sciences Division, Earth System Research Laboratory, NOAA, Boulder, Colorado, USA.
[8]Formerly at Chemical Sciences Division, Earth System Research Laboratory, NOAA, Boulder, Colorado, USA.
[9]Formerly at Atmospheric Chemistry Division, National Center for Atmospheric Research, Boulder, Colorado, USA.
[10]Atmospheric Chemistry Division, National Center for Atmospheric Research, Boulder, Colorado, USA.

0148-0227/06/2005JD006680$09.00

tions of NO_2 columns provides additional constraints that could yield an improved NO_x emission inventory and an improved representation of processes affecting NO_x.

[3] Bottom-up NO_x emission inventories for a specific year quickly could become outdated in a rapidly industrializing economy. An increase in global NO_x emissions of more than 50% is expected over 2000–2020 [*Intergovernmental Panel on Climate Change*, 2001] with most of this increase from Asia. Rising Asian emissions may have implications for radiative forcing by tropospheric ozone [*Berntsen et al.*, 1997; *Brasseur et al.*, 1998; *Wild et al.*, 2001] and for surface air quality throughout the Northern Hemisphere [*Jacob et al.*, 1999; *Fiore et al.*, 2002; *Lelieveld et al.*, 2002; *Derwent et al.*, 2004]. Global numerical models rely on current information for simulation of atmospheric composition and for climate change assessments. Space-based measurements provide timely information that could be used to more accurately reflect current emissions.

[4] The SCanning Imaging Absorption spectroMeter for Atmospheric CHartographY (SCIAMACHY) instrument onboard the ENVISAT satellite provides the capability for global measurement of atmospheric NO_2 columns through observation of global backscatter [*Bovensmann et al.*, 1999]. The satellite was launched in March 2002 into a sun-synchronous orbit, crossing the equator at 1000 local time in the descending node. The SCIAMACHY instrument observes the atmosphere in the nadir view with a typical surface spatial resolution of 30 km along track by 60 km across track. Global coverage is achieved every 6 days. An advantage of SCIAMACHY over the earlier Global Ozone Monitoring Experiment (GOME) satellite instrument [*European Space Agency*, 1995; *Burrows et al.*, 1999] is that the surface spatial resolution of SCIAMACHY is seven times higher than that of GOME. The higher resolution is expected to reduce the retrieval error by reducing subpixel variation, especially from clouds. The close relationship between tropospheric NO_2 columns and land surface NO_x emissions has been previously demonstrated with GOME observations [*Leue et al.*, 2001; *Beirle et al.*, 2003; *Martin et al.*, 2003b; *Jaeglé et al.*, 2005; *Müller and Stavrakou*, 2005]. Here we apply the higher resolution SCIAMACHY measurements to produce an improved NO_x emission inventory.

[5] A prerequisite for this analysis is an understanding of the accuracy of the SCIAMACHY retrieval, and of the emission inventory. We focus on the summer of 2004 during which the International Consortium for Atmospheric Research on Transport and Transformation (ICARTT) aircraft campaign occurred over eastern North America and the North Atlantic Ocean. Section 2 describes the numerical model used in our analysis. In section 3 we retrieve tropospheric NO_2 columns from SCIAMACHY as our top-down constraint and validate the retrieval with airborne measurements of NO_2. Section 4 presents the a posteriori NO_x emission inventory and evaluates it with airborne measurements. The a posteriori is compared with independent bottom-up inventories in section 5.

2. Global Chemical Transport Model

[6] We use the GEOS-Chem global 3-D model of atmospheric composition to provide NO_2 profiles to constrain the SCIAMACHY retrieval as described in section 3.1, to conduct a simple inversion to infer NO_x emissions from the observed NO_2 columns as described in section 4.1, and to serve as an intermediary to compare the a priori and a posteriori NO_x emission inventories with airborne in situ observations as described in section 4.3. The simulation is driven by assimilated meteorological data from the Goddard Earth Observing System (GEOS-4) at the NASA Global Modeling and Assimilation Office (GMAO). The data have 6-hour temporal resolution (3-hour resolution for surface variables and mixing depths) and $1^\circ \times 1.25^\circ$ horizontal resolution. There are 55 hybrid eta vertical levels, extending from the surface to 0.01 hPa. The lowest 2 km is resolved by five layers with midpoints at 60, 250, 620, 1200, and 1990 m altitude for a column based at sea level. We use version 7-01-02 of GEOS-Chem (www-as.harvard.edu/chemistry/trop/geos) at $2^\circ \times 2.5^\circ$ horizontal resolution with updated midlatitude lightning NO_x emissions as described below.

[7] The GEOS-Chem model includes a detailed simulation of tropospheric ozone-NO_x-hydrocarbon chemistry as well as of aerosols and their precursors using 41 tracers, ~90 species, and ~300 reactions. The ozone-NO_x-hydrocarbon simulation was first described by *Bey et al.* [2001] with updates by *Fiore et al.* [2002] and *Martin et al.* [2002a, 2003a]. The model presently includes sulfate, nitrate, ammonium, black carbon, organic carbon, mineral dust, and sea salt [*Park et al.*, 2003, 2004; *Alexander et al.*, 2005; *Park et al.*, 2005]. The aerosol and gaseous simulations are coupled through formation of sulfate and nitrate, $HNO_3(g)/NO_3^-$ partitioning of total inorganic nitrate, heterogeneous chemistry on aerosols [*Jacob*, 2000; *Evans and Jacob*, 2005], and aerosol effects on photolysis rates [*Martin et al.*, 2003a]. Simulation of wet and dry deposition follows the schemes developed by *Bey et al.* [2001]; extension to moderately soluble gases with low retention efficiencies upon cloud freezing is as described by *Park et al.* [2004].

[8] Table 1 contains the annual global NO_x emissions in GEOS-Chem for all sources. Anthropogenic NO_x emissions are from the Global Emission Inventory Activity (GEIA) [*Benkovitz et al.*, 1996] and scaled by country based on energy statistics to 1998 (the last year of available statistics) as described by *Bey et al.* [2001]. Time-of-day and day-of-the-week variation are based on work of *Environmental Protection Agency* [1989] as described by *Jacob et al.* [1993]. Soil NO_x emissions are computed using a modified version of the algorithm of *Yienger and Levy* [1995] with the canopy reduction factors described by *Wang et al.* [1998]. The climatological biomass burning inventory is seasonally varying and is based on satellite observations of fires over 1996–2000 from the Along Track Scanning Radiometer (ATSR) as derived by *Duncan et al.* [2003]. Emissions of lightning NO_x are linked to deep convection following the parameterization of *Price and Rind* [1992] with vertical profiles from *Pickering et al.* [1998] as implemented by *Wang et al.* [1998]. The magnitude of the tropical source is constrained to reproduce ozone observations as described by *Martin et al.* [2002a]. Northern midlatitude lightning NO_x emissions are increased here by a factor of 4 to 1.6 Tg N yr^{-1} for consistency with aircraft observations as described in section 3.2. The resulting ratio of midlatitude to tropical lightning NO_x emissions is more

Table 1. A Priori Annual Global GEOS-Chem NO_x Emissions

Source	Emissions, Tg N
Fossil fuel combustion[a]	23.3 (11.5)[b]
Lightning	7.1 (4.2)
Biomass burning	6.0 (3.7)
Soils	7.1 (3.5)
Biofuels	2.2 (1.1)
Aircraft	0.5 (0.26)
Stratosphere	0.1[c] (0.05)

[a]Fossil fuel emissions are based on GEIA and scaled to 1998.
[b]Values for May–October are given in parentheses.
[c]The cross-tropopause NO_y flux is 0.5 Tg N yr^{-1} (including 0.1 Tg N yr^{-1} as NO_x and 0.4 Tg N yr^{-1} as HNO_3).

consistent with the ratio of midlatitude to tropical lightning flashes of 22% determined by *Christian et al.* [2003] using space-based observations from the Optical Transient Detector.

3. SCIAMACHY Tropospheric NO_2 Retrieval

3.1. Retrieval Algorithm

[9] Our retrieval of tropospheric NO_2 columns presented here is based on the algorithms of *Martin et al.* [2002b, 2003b]. We focus on May–October 2004, a time period that brackets the ICARTT campaign, but extend the retrieval to April 2005 to span an entire year. Level-1 SCIAMACHY data for January–April 2004 were not available to us at the time.

[10] Following *Chance* [1998] and *Martin et al.* [2002b] we determine total slant columns of NO_2 by directly fitting backscattered radiance spectra observed by SCIAMACHY. The spectral fit is optimized for SCIAMACHY over the wavelength region 429–452 nm using measured reference spectra for NO_2 at 243 K [*Bogumil et al.*, 2003], ozone at 223K [*Bogumil et al.*, 2003], H_2O at 296 K [*Rothman et al.*, 1998], O_2-O_2 at 296 K [*Greenblatt et al.*, 1990], and the Ring effect [*Chance and Spurr*, 1997]. The solar spectra for each orbit are from the elevation scan mirror on the SCIAMACHY instrument. We find no evidence of a diffuser plate artifact [*Richter and Wagner*, 2001; *Martin et al.*, 2002b] that complicated retrievals of NO_2 from GOME. The stratospheric column and instrument biases are removed by assuming that NO_2 over the central Pacific is mainly stratospheric, subtracting the corresponding columns from the ensemble of SCIAMACHY observations for the appropriate latitude and month, and correcting the result for the small amount of tropospheric NO_2 over the Pacific. The stratospheric column is taken to be zonally invariant; this assumption does not cause significant error in summer [*Martin et al.*, 2002b], but is questionable at high latitudes in other seasons owing to dynamical variability [*Boersma et al.*, 2004].

[11] We apply the air mass factor (AMF) formulation of *Palmer et al.* [2001] to convert the resulting tropospheric slant columns into vertical columns. This formulation computes the AMF as the integral over the tropospheric column of the relative vertical distribution of NO_2 (shape factor) weighted by the local sensitivity to NO_2 of the solar radiation backscattered to space (scattering weights). The temperature dependence of the NO_2 cross section is accounted for using local GEOS-4 temperature profiles for every SCIAMACHY scene. The shape factor for every SCIAMACHY scene is specified from a GEOS-Chem model simulation of that scene, while the scattering weights are calculated from the Linearized Discrete Ordinate Radiative Transfer (LIDORT) model [*Spurr et al.*, 2001; *Spurr*, 2002]. Prior evaluation of the NO_2 shape factor with in situ airborne measurements in the lower troposphere over the southeast United States found agreement to within 20%; differences would affect the retrieved NO_2 columns by only a few percent [*Martin et al.*, 2004]. Monthly varying surface reflectivity fields are from *Koelemeijer et al.* [2003]. Our aerosol correction uses daily local aerosol profiles from the GEOS-Chem simulation for that scene as described by *Martin et al.* [2003b].

[12] Our cloud correction in the AMF uses cloud top pressure and cloud fraction information from the Fast Retrieval Scheme for Cloud Observables (FRESCO) [*Koelemeijer et al.*, 2002] algorithm. For consistency with FRESCO, clouds are treated as Lambertian surfaces here rather than as a collection of Mie scatterers as was possible in our GOME retrieval [*Martin et al.*, 2002b]. We exclude scenes in which the cloud radiance fraction is more than 50%; that is, more than half of the backscattered intensity is from the cloudy-sky fraction of the scene as determined from the radiative transfer calculation constrained with the local cloud information.

[13] *Martin et al.* [2002b, 2003b] and *Boersma et al.* [2004] estimated that the total uncertainty in the GOME retrieval of tropospheric NO_2 columns over continental source regions is largely determined by the AMF calculation due primarily to surface reflectivity, clouds, aerosols, and the trace gas profile. The uncertainty in each measurement exhibits large spatial variation [*Boersma et al.*, 2004]. The higher spatial resolution of SCIAMACHY over GOME is expected to reduce uncertainty in the AMF calculation due to reduction in subpixel variability, especially from clouds. However, we conservatively adopt the same uncertainty estimate in the AMF as with GOME owing to additional concern about the treatment of clouds as Lambertian surfaces in the SCIAMACHY AMF calculation. We estimate the typical 1-sigma uncertainty for each SCIAMACHY measurement is 40% due to the AMF plus an absolute component of 1×10^{15} molecules cm^{-2} from spectral fitting and subtraction of the stratospheric NO_2 column. Our estimate for the monthly mean uncertainty is $\pm(5 \times 10^{14}$ molecules cm^{-2} + 30%) which could include systematic errors.

3.2. Evaluation of NO_2 Profiles Used in the Retrieval; Sensitivity to Lightning

[14] We validate our retrieval using coincident airborne in situ measurements as part of the ICARTT campaign. Figure 1 shows the flight tracks of the NASA DC-8 and NOAA WP-3D aircraft which spanned conditions from remote marine to highly polluted. The DC-8 sampled more remote regions than the WP-3D. NO_2 was measured on the DC-8 by laser induced fluorescence [*Thornton et al.*, 2000] and on the WP-3D by photolysis of NO_2 and chemiluminescence detection of the product NO [*Ryerson et al.*, 2003].

[15] As discussed above, independent information on the relative NO_2 vertical profile is necessary for determination

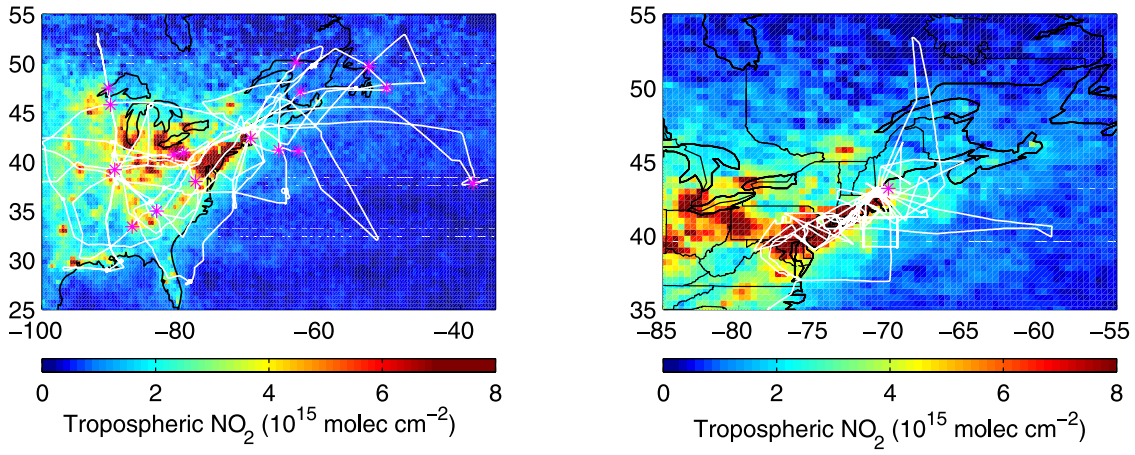

Figure 1. Tropospheric NO_2 columns retrieved from the SCIAMACHY satellite instrument for May–October 2004. White lines show flight tracks of the (left) DC-8 and (right) WP-3D aircraft. Magenta stars indicate the location of coincident aircraft and SCIAMACHY measurements used for validation.

of column abundance from SCIAMACHY. Figure 2 compares campaign-average profiles of NO_2 measured from aircraft with those calculated with the GEOS-Chem model. Here and elsewhere, model results are sampled along the flight tracks at the measurement time. Observations are averaged over model grid boxes. The aircraft and model profiles are generally consistent in the lower troposphere. However, the standard simulation with 0.4 Tg N yr^{-1} of lightning from northern midlatitudes (north of 30°N) underestimates NO_2 in the upper troposphere by 100 pptv. The AMFs calculated with the simulated profiles are lower than the AMFs calculated from the campaign-average in situ DC-8 profiles by 12% over land and 9% over ocean. We find no bias in the comparison of measured and simulated profiles of CO, providing evidence that the upper tropospheric bias in NO_2 is indeed from lightning and not convection. R. Hudman et al. (A multi-platform analysis of the North American reactive nitrogen budget during the ICARTT summer intensive, manuscript in preparation, 2006) (hereinafter referred to as Hudman et al., manuscript in preparation, 2006) evaluated the GEOS-Chem simulation with in situ measurements of CO_2 and NO_y from the DC-8 and find little evidence for a model underestimate in aircraft NO_x emissions.

[16] We conduct an additional simulation with enhanced northern midlatitude lightning NO_x emissions (1.6 Tg N yr^{-1}). Tropical lightning NO_x emissions remain unchanged. Figure 2 shows that the simulation with enhanced midlatitude lightning reduces the model underestimate of NO_2 in the upper troposphere by more than a factor of 2, but introduces a positive bias of 20 pptv in the middle troposphere. The remaining bias in the model vertical placement of lightning NO_x may be explained by low cloud top heights in the GEOS-4 meteorological fields (Hudman et al., manuscript in preparation, 2006), or by an underestimate in NO_x emissions from intracloud discharges; *Fehr et al.* [2004] and *DeCaria et al.* [2005] compared aircraft NO_x measurements with a three-dimensional cloud model and

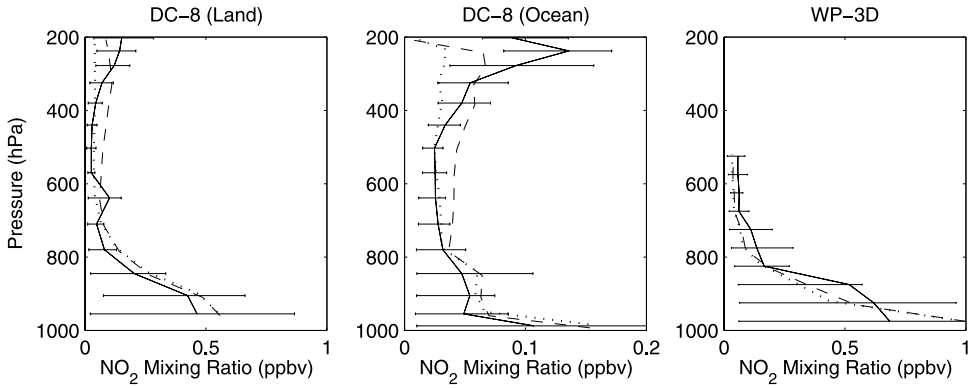

Figure 2. Vertical profiles of NO_2 over eastern North America averaged over the entire ICARTT campaign. In situ measurements (solid lines) are compared with a GEOS-Chem simulation with 1.6 Tg N yr^{-1} from northern midlatitude lightning (dashed lines) and a sensitivity simulation with 0.4 Tg N yr^{-1} from northern midlatitudes lightning (dotted lines). Horizontal bars represent 17th and 83rd percentiles of the measurements.

Table 2. Characteristics of Measurements Used for Validation

Date	Latitude, deg	Longitude, deg	SCIAMACHY Time, UTC	Aircraft Time, UTC	Aircraft Altitude, km
8 July	38.0	−78.0[a]	1515	1946–2011	0.4–3.2
10 July	40.7	−81.1	1558	1532–1547	0.7–5.8
10 July	40.9	−79.7	1558	1547–1621	0.7–10.6
10 July	35.0	−83.6	1600	1822–1859	0.9–11.4
10 July	33.4	−87.1	1600	1911–1939	0.4–11.3
12 July	39.2	−89.6	1636	1509–1528	0.7–6.4
12 July	45.8	−90.2	1634	1622–1656	0.7–10.5
15 July	47.5	−90.5	1639	1456–1520	0.5–9.7
18 July	47.1	−63.0	1505	1441–1514	0.3–10.0
22 July	50.1	−63.6	1438	1840–1911	0.5–9.2
28 July	37.8	−38.2	1312	1658–1728	0.3–9.0
31 July	42.4	−70.1	1457	1459–1514	0.4–6.8
31 July	41.2	−66.1	1457	1600–1632	0.3–9.4
31 July	41.1	−63.3	1457	1642–1705	0.3–9.1
31 July	43.2	−70.1[b]	1457	2125–2136	0.04–3.6
2 Aug	49.7	−53.1	1352	1740–1755	0.3–6.6
2 Aug	47.5	−50.6	1352	1811–1831	0.3–7.9

[a]Locations correspond to the center of the SCIAMACHY pixel.
[b]Airborne measurements at this location are from the WP-3D aircraft. All other locations were sampled from the DC-8 aircraft.

concluded that intracloud lightning discharges are more energetic than derived by *Price et al.* [1997] as implemented in GEOS-Chem using profiles from *Pickering et al.* [1998]. The biases in the AMF calculated with the simulated profiles, versus the AMF calculated from the campaign-averaged in situ profiles, are reduced to 1% over land and 5% over ocean using the simulation with enhanced lightning. We use the simulation with 1.6 Tg N yr^{-1} from northern midlatitude lightning in our SCIAMACHY retrieval.

3.3. Validation of Retrieved NO_2 Columns With in Situ Measurements

[17] Table 2 contains the characteristics of the satellite and airborne measurements used here for validation. Several dedicated aircraft spirals were conducted during SCIAMACHY overpasses for validation purposes. Additional comparisons of opportunity also are considered if they satisfy the following coincidence criteria. Daytime measurements must occur within a SCIAMACHY scene on the date of observation; the two measurements were usually within hours of each other. Many WP-3D measurements were at night and excluded from the comparison. The in situ measurements must sample the lower troposphere below 1 km and up to at least 3 km. Over regions with enhanced NO_2 ($>3 \times 10^{15}$ molecules cm^{-2}), which likely have spatially heterogeneous surface sources, in situ measurements must be taken within 15 km of the center of the SCIAMACHY pixel. Nearly 20 coincident measurements are found, providing an unprecedented opportunity to validate SCIAMACHY retrievals.

[18] Partial columns are calculated from the airborne measurements by integrating the average NO_2 number density from the surface to the highest measurement altitude. The vertical step size is 700 m for the WP-3D measurements and 1000 m for the DC-8. The larger step size for the DC-8 accommodates its infrequent altitude below 700 m. The partial tropospheric column above the highest measurement altitude of an individual profile is determined by integrating a mean profile determined from the average NO_2 measured on all DC-8 flights over eastern North America and the North Atlantic Ocean that were coincident with a SCIAMACHY measurement.

[19] Figure 3 compares tropospheric NO_2 columns retrieved from SCIAMACHY with those determined with in situ measurements. The geometric mean in situ to SCIAMACHY ratio m is 0.82 with a geometric standard deviation σ of 1.69 (i.e., 67% of the values are between m/σ and $m\sigma$). The coefficient of determination, r^2, is 0.60. The slope of the reduced-major axis regression line is 0.82. The two measurement techniques are consistent within their uncertainty. However, the comparison exhibits modest scatter that likely is related to incomplete sampling of the entire vertical column and of the potentially heterogeneous lower mixed layer. Columns calculated from in situ measurements tend to be lower than those determined from SCIAMACHY over remote regions, and higher over regions with enhanced NO_2. A similar degree of consistency was found during a previous SCIAMACHY validation exercise over southern Europe [*Heue et al.*, 2005].

3.4. Retrieved NO_2 Columns

[20] Figure 4 shows tropospheric NO_2 vertical columns retrieved from SCIAMACHY for May 2004 to April 2005. Pronounced enhancements are apparent over major industrial and metropolitan areas. The high spatial heterogeneity in regions with distinct sources, such as the southwestern United States and the Middle East, provides empirical evidence of the short NO_x lifetime that facilitates mapping of NO_2 columns onto NO_x emissions. Moderate enhancements are found in central Africa from biomass burning [*Richter and Burrows*, 2002]. An enhancement of comparable magnitude is observed over northern equatorial Africa with a maximum at the beginning of the rainy season in early June that *Jaeglé et al.* [2004] attributed to rain-induced soil NO_x emissions. There are weak enhancements along ocean ship tracks near Kuala Lumpur [*Beirle et al.*, 2004b; *Richter et al.*, 2004].

[21] Tropospheric NO_2 columns are more sensitive to NO_x in the lower troposphere than in the upper troposphere

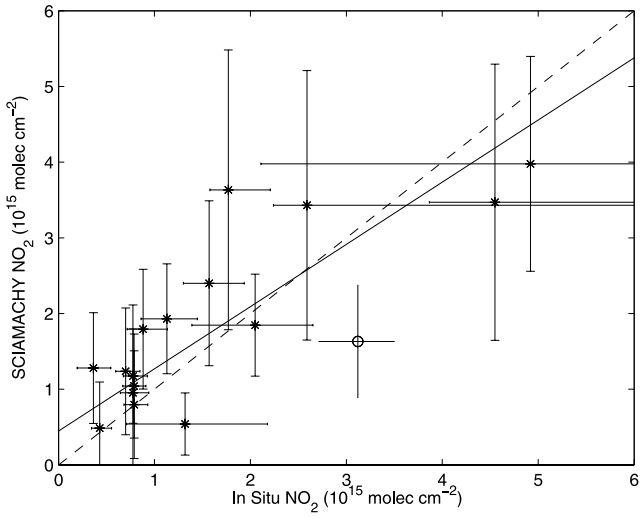

Figure 3. Comparison of coincident NO_2 columns retrieved from SCIAMACHY with those determined from in situ measurements on the WP-3D (circle) and DC-8 (stars) aircraft. Vertical lines indicate the SCIAMACHY retrieval uncertainty. Horizontal lines are determined by summing vertically in quadrature the difference between the mean and the 17th and 83rd percentiles of in situ measurements. The dashed line represents the y = x line. The solid line was calculated with reduced major-axis linear regression [*Hirsch and Gilroy*, 1984].

[*Martin et al.*, 2002b]. This sensitivity is due largely to the large decrease in the NO_2/NO_x ratio with increasing altitude that is driven the temperature dependence of the NO + O_3 reaction. However, there is mounting evidence of a lightning NO_x signal in GOME observations of tropospheric NO_2 [*Richter and Burrows*, 2002; *Edwards et al.*, 2003; *Beirle et al.*, 2004a, 2005; *Boersma et al.*, 2005; *Choi et al.*, 2005]. Figure 2 indicates that North American lightning NO_x emissions make a larger relative contribution to the mean NO_2 column over ocean than over land. Close inspection of our SCIAMACHY NO_2 columns during summer reveals a weak plume from North American lightning NO_x emissions that extends across the North Atlantic Ocean to Europe.

[22] Figure 5 shows retrieved and simulated NO_2 columns over the North Atlantic Ocean during May–October 2004. The SCIAMACHY NO_2 columns are near the detection limit of 5×10^{14} molecules cm^{-2}. The spatial extent of the NO_2 plume in the SCIAMACHY observations implies the enhancement is in the upper troposphere where the NO_x lifetime of a week is sufficient for long-range transport. The feature persists if a more strict cloud filter is applied to the SCIAMACHY NO_2 measurements. The GEOS-Chem simulation with 0.4 Tg N yr^{-1} from midlatitude lightning shows little enhancement. Indeed, the underestimate in that simulation with respect to in situ measurements of upper tropospheric NO_2 was attributed to an underestimate in lightning NO_x emissions in section 3.2. The simulation with 1.6 Tg N yr^{-1} better simulates the NO_2 plume in the SCIAMACHY observations, but does not capture its magnitude nor spatial extent. The remaining bias likely arises from insufficient altitude of lightning NO_x emissions which

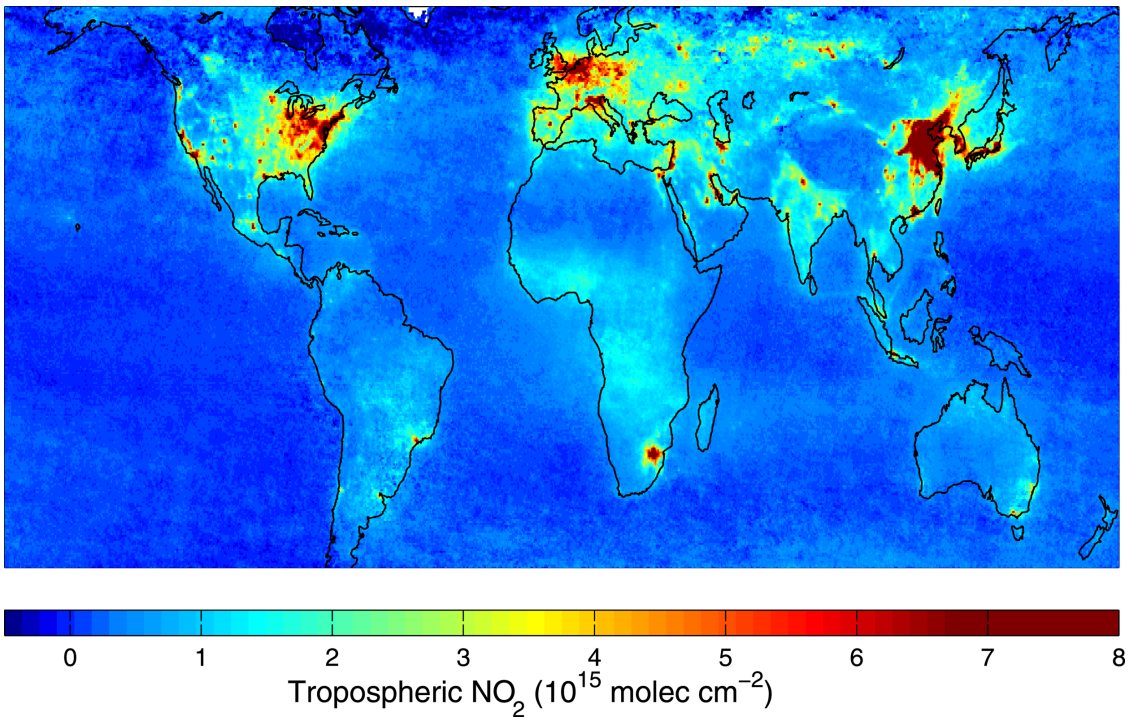

Figure 4. Mean tropospheric NO_2 columns retrieved from the SCIAMACHY satellite instrument for May 2004 to April 2005. Scenes where clouds or snow dominate solar backscatter have been excluded from the average to reduce retrieval uncertainty.

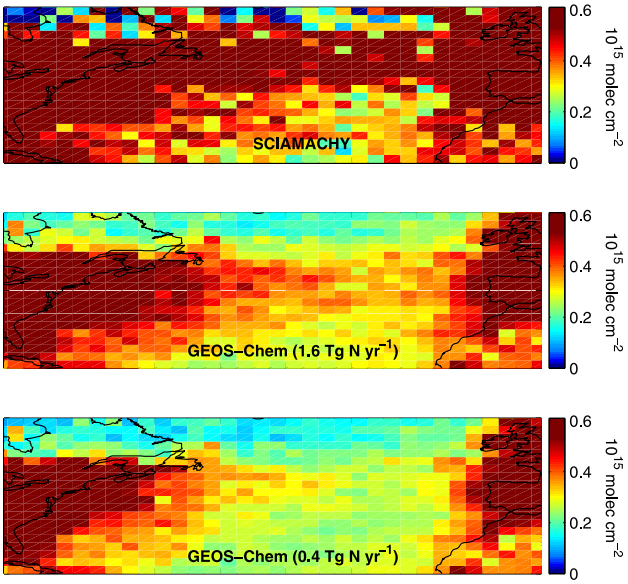

Figure 5. Tropospheric NO_2 columns over the North Atlantic Ocean averaged over May–October 2004 as (top) retrieved from SCIAMACHY, (middle) calculated with the GEOS-Chem model using 1.6 Tg N yr^{-1} from lightning at northern midlatitudes, and (bottom) calculated with the GEOS-Chem model using 0.4 Tg N yr^{-1} from lightning at northern midlatitudes. Scenes where clouds or snow dominate SCIAMACHY observations of solar backscatter have been excluded from the average to reduce retrieval uncertainty.

would decrease the NO_x lifetime and the spatial extent of the plume, consistent with our interpretation from comparison with the DC-8 measurements. Hudman et al. (manuscript in preparation, 2006) further investigate this issue in the GEOS-Chem simulation.

4. A Posteriori NO_x Emission Inventory

4.1. Approach to Produce the A Posteriori Inventory

[23] Following *Martin et al.* [2003b], we determine the local top-down surface NO_x emissions E_t for May 2004 to April 2005 from the local retrieved NO_2 columns Ω_r through the following linear relationship:

$$E_t = \alpha\, \Omega_r, \tag{1}$$

where the coefficient $\alpha = (\Omega_{NOx}/\Omega_{NO2})/\tau_{NOx}$ is determined with the GEOS-Chem chemical mechanism by sampling the model at the SCIAMACHY observation time using the simulation with a priori emissions $\alpha = E_a/\Omega_a$. This simple approach yields an effective NO_x lifetime τ_{NOx} that accounts for local NO_x chemistry, NO_x transport, and a $\Omega_{NOx}/\Omega_{NO2}$ ratio that accounts for free tropospheric NO_x sources as represented by the GEOS-Chem model. This approach takes advantage of the short NO_x lifetime in the lower mixed layer of less than a day that is inferred from in situ measurements [*Ryerson et al.*, 2003] and expected from model calculations during most of the year [*Martin et al.*, 2003b]. For a horizontal wind speed of 10 m/s, the corresponding smearing length scale [*Palmer et al.*, 2003] ranges from 50 km in summer to 250 km in winter, comparable to the scale of the model grid. The SCIAMACHY data are regridded to the GEOS-Chem resolution before application of equation (1). We apply equation (1) only over land and coastal regions. Inference of oceanic surface NO_x emissions would be prone to excessive error due to the large relative contribution of lightning to the NO_2 column over ocean as apparent in Figures 2 and 5.

[24] A possible concern is the degree of nonlinearity in the relationship between the rate of surface NO_x emissions and the NO_2 column over a range of NO_x emissions. NO_x concentrations respond nonlinearly to changes in emissions due to feedbacks on OH [*Kunhikrishnan and Lawrence*, 2004]. However, NO_2 would be expected to respond more linearly than NO_x to changes in emissions owing to compensation in the NO_2/NO_x ratio that results from feedbacks on hydroxyl radicals and O_3. We quantify the combination of these two effects with the GEOS-Chem model.

[25] Figure 6 shows the simulated NO_2 column as a function of the NO_x emission rate for December and July at six different locations. The slope of the line indicates the local value of α in equation (1). The greater slope in winter is due to the longer NO_x lifetime. Biomass burning emissions in January contribute to the large seasonal variation in Nigeria. The exact calculations indicated by circles and stars show highly linear relationships that are consistent to within 10% of the local relationship used in equation (1). A simulation at higher spatial resolution should better account for spatial variation in the relationship between NO_2 columns and NO_x emissions, and may yield a more nonlinear relationship over urban areas.

[26] Table 3 provides regional and global totals in the top-down inventory. Global top-down NO_x emissions are 46% higher than the a priori. The largest regional increase (6.0 Tg N yr^{-1}) is found in East Asia. We further investigate these differences in the next section.

[27] The a posteriori inventory E is calculated from the top-down and bottom-up inventories, weighting by their relative uncertainty. Assuming a lognormal distribution of errors in the a priori ε_a and top-down ε_t yields

$$\ln E = \frac{(\ln E_t)(\ln \varepsilon_a)^2 + (\ln E_a)(\ln \varepsilon_t)^2}{(\ln \varepsilon_a)^2 + (\ln \varepsilon_t)^2}, \tag{2}$$

with a corresponding relative error ε

$$(\ln \varepsilon)^{-2} = (\ln \varepsilon_a)^{-2} + (\ln \varepsilon_t)^{-2}. \tag{3}$$

[28] We calculate the total uncertainty in the top-down emission inventory by adding in quadrature the uncertainty in the NO_2 retrieval, in the calculation of α, and in the representativeness of α. Section 3.1 described the uncertainty in the NO_2 retrieval of $\pm(5 \times 10^{14}$ molecules cm^{-2} + 30%). Previous comparison of the GEOS-Chem simulations of the NO_x/NO_y ratio over and downwind of North America [*Fiore et al.*, 2002; *Li et al.*, 2004; Hudman et al., manuscript in preparation, 2006] and East Asia [*Wang et al.*, 2004] suggests that the uncertainty in the calculation of α is 30%. We add in quadrature an additional 10% error for the representativeness of α based on the comparison in Figure 6.

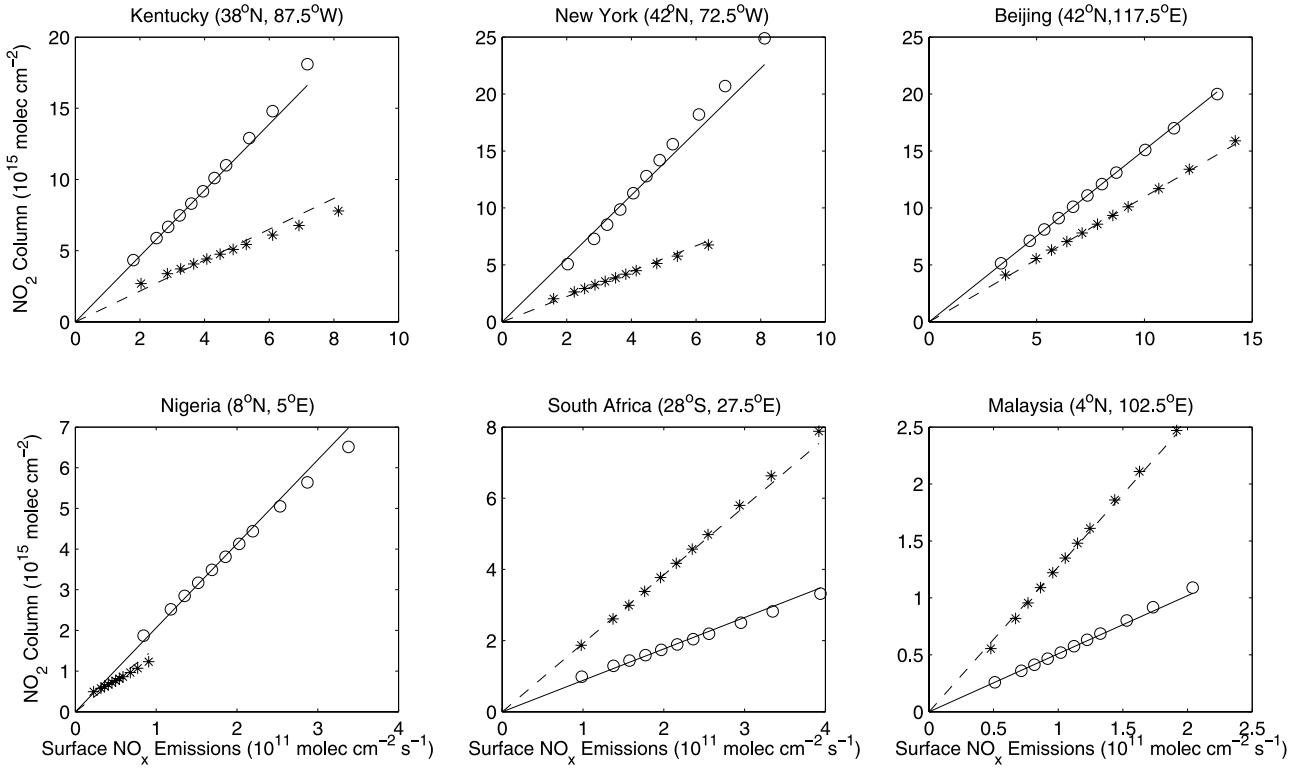

Figure 6. Local relationship between modeled NO_2 columns and NO_x emissions at six different locations at 1000 local time during January (solid lines and circles) and July (dashed lines and stars). Lines show the linear relationship used in equation (1) to infer top-down NO_x emissions from retrieved NO_2 columns. Circles and stars show the NO_2 column calculated with sensitivity simulations in which surface NO_x emissions were varied within a factor of 2 of the standard simulation.

The total uncertainty in the top-down inventory is less than 50% over regions with enhanced NO_2 and increases to more than a factor of 2 over remote regions.

[29] The uncertainty in the a priori inventory is not available. The uncertainty in biomass burning and soil NO_x emissions is taken to be a factor of 3, reflecting the range of global estimates [*Prather et al.*, 2001]. We estimate the local uncertainty in the fossil fuel inventory based on comparison with the recently available EDGAR 3.2FT2000 inventory [*Olivier et al.*, 2005]; values are about 50% over major industrial areas and higher elsewhere similar to *Martin et al.* [2003b]. An additional 10% error is applied here to reflect the outdated a priori; our resultant a posteriori inventory increases by 0.2 Tg N yr^{-1} as a result of the decreased weighting of the bottom-up inventory compared with the top-down inventory. Similarly, an additional 30% error is applied here to Chinese emissions in light of potentially unrepresented sources inferred from aircraft

Table 3. Annual Mean Regional NO_x Emissions (and Relative Errors)[a]

	A Priori	SCIAMACHY	A Posteriori	EDGAR[b]	M2003[c]	J2005[d]
East Asia	6.7 (2.8)	12.7 (1.6)	9.8 (1.7)	8.2	7.3	7.6
North America	8.0 (1.9)	9.7 (1.6)	8.7 (1.5)	7.3	8.4	8.5
Europe	6.4 (2.1)	10.2 (1.5)	8.2 (1.5)	9.2	7.2	7.0
Africa	6.9 (2.5)	9.2 (1.8)	8.1 (1.7)	7.8	7.4	8.5
SE Asia and India	4.8 (2.3)	5.5 (1.9)	4.7 (1.7)	4.6	3.4	3.6
South America	4.0 (2.5)	5.3 (2.1)	4.7 (1.8)	4.9	3.2	3.7
Australia	1.1 (2.7)	2.8 (2.0)	1.9 (1.8)	1.2	1.0	1.2
Total	37.9 (2.3)	55.4 (1.8)	46.1 (1.6)	43.2	37.7	40.1

[a]Units are Tg N yr^{-1}. Relative errors represent the geometric standard deviation about the mean. Region boundaries follow standard convention. Emissions include all land surface sources (fossil fuel combustion, biofuels, biomass burning, and soils) and exclude nonsurface sources (lightning, aircraft, and stratosphere).

[b]The EDGAR 3.2FT2000 inventory only includes fossil fuel, biomass burning, and biofuel emissions. We add the GEOS-Chem soil NO_x emissions here for consistency.

[c]A posteriori emission inventory is from *Martin et al.* [2003b] based on GOME 1996–1997 NO_2 columns.

[d]A posteriori emission inventory is from *Jaeglé et al.* [2005] based on GOME 2000 NO_2 columns.

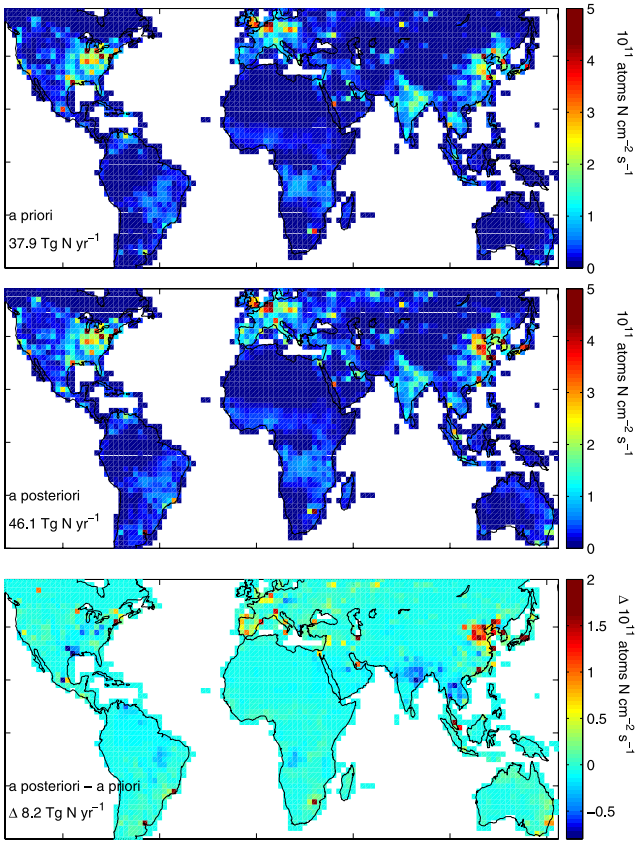

Figure 7. Average NO_x emissions at 2° × 2.5° horizontal resolution for the (top) a priori and (middle) a posteriori inventories. Only surface NO_x emissions are included; nonsurface emissions from lightning, aircraft, and the stratosphere are excluded. Annual global emissions are indicated in the bottom left. (bottom) Difference between the a posteriori and a priori inventories.

and surface measurements by *Wang et al.* [2004]; our resultant a posteriori inventory increases by 0.4 Tg N yr^{-1}.

[30] Table 3 provides regional and global uncertainties. The global relative uncertainty in the top-down inventory is a factor of 2.3, compared with a factor of 1.8 in the a priori, resulting in more influence from SCIAMACHY than the bottom-up inventory in the calculation of the a posteriori.

4.2. Discussion of the A Posteriori Inventory

[31] Figure 7 shows the a priori and a posteriori inventories of land surface emissions. Land surface emissions here include contributions from fossil fuels, biofuels, biomass burning, and soils; they exclude contributions from lightning, aircraft, or the stratosphere. The global total of the a posteriori (46.1 Tg N yr^{-1}) is 22% higher than the a priori. The two inventories exhibit a high degree of consistency ($r^2 = 0.81$). We find little evidence of horizontal smearing in the a posteriori inventory which should be most apparent at high latitudes along prevailing wind directions.

[32] Table 3 provides regional totals. A posteriori emissions from East Asia exceed those from either North America or Europe. Soils and biomass burning explain most of Africa's relatively large surface emissions [*Jaeglé et al.*, 2005]. The estimate of the global uncertainty in NO_x emissions is reduced from a factor of 2.3 in the a priori to a factor of 1.6 in the a posteriori as calculated with equation (3).

[33] The bottom panel of Figure 7 shows the difference between the a priori and a posteriori inventories. Most regions of the world exhibit little change. However, pronounced differences in NO_x emissions are apparent over numerous major industrial areas including Beijing, Tokyo, Buenos Aires, and New York City. The a posteriori is a factor of 2 larger than the a priori for Shanghai, Hong Kong, Tehran, and Sao Paolo. Discrepancies were noted in many of these regions in a previous comparison of the a priori with GOME [*Martin et al.*, 2003b], although less clearly owing to its coarse spatial resolution. Regions with annual mean emissions of more than 2×10^{11} molecules cm^{-2} s^{-1} account for 40% of the difference between the a priori and a posteriori inventories. The comparison of NO_2 columns determined from SCIAMACHY and in situ measurements in Figure 3 suggests that NO_x emissions could be even higher over megacities. The biases found here reflect a combination of imperfect information in the GEIA inventory, and recent changes in emissions unaccounted for in the a priori. Rapid growth of the Asian transportation sector is leading to a rapid rise in NO_x emissions [*Akimoto*, 2003; *Streets et al.*, 2003]. Oil consumption by the Chinese road transport system increased at an average annual growth rate of 9% over 1997–2002 [*He et al.*, 2005]. *Richter et al.* [2005] examined trends in tropospheric NO_2 columns from GOME and found an increase of 50% over industrial China during 1996–2002, with an accelerating increase in latter years. In contrast, a posteriori emissions from the Ohio River Valley of the United States are 10–25% lower than the a priori as expected from controls on NO_x emissions from electric utilities [*Environmental Protection Agency*, 2003] and by trends in GOME NO_2 columns [*Richter et al.*, 2005]. Modest decreases in the a posteriori with respect to the a priori are found over biomass burning regions of South America, Central Africa, and South Asia, consistent with previous inversions [*Martin et al.*, 2003b; *Jaeglé et al.*, 2005; *Müller and Stavrakou*, 2005].

[34] Figure 8 shows the seasonal variation in the a posteriori inventory. A posteriori NO_x emissions in the southern tropics are most intense during May–October, and in the northern tropics during November–April, as expected from satellite observations of fires [*Duncan et*

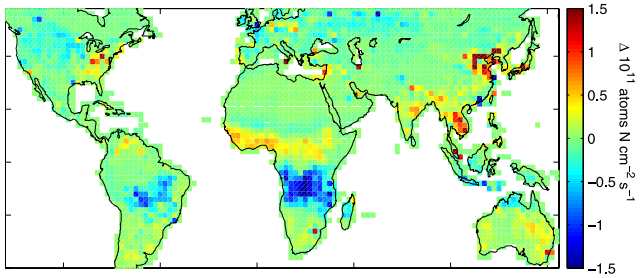

Figure 8. Seasonal change in a posteriori NO_x emissions as determined for November 2004 to April 2005 minus May–October 2004.

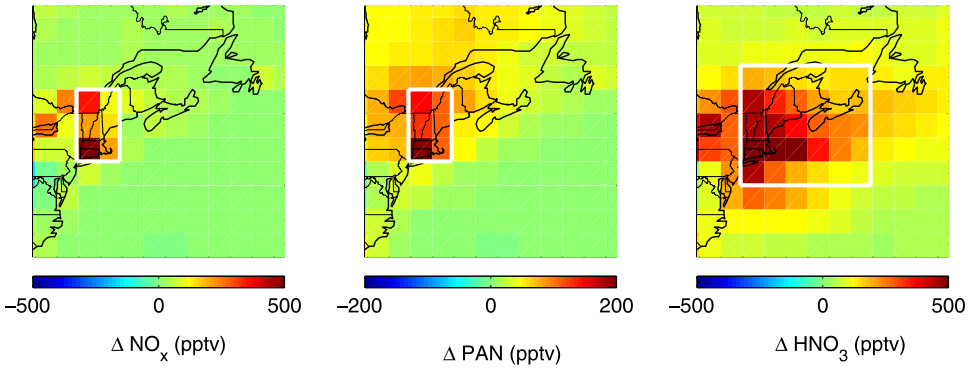

Figure 9. Difference in the GEOS-Chem model simulation of NO_x, PAN, and HNO_3 over the period 5 July 2004 to 15 August 2004 in the lower troposphere (~600 m) using the a posteriori inventory minus the simulation using the a priori inventory. White boxes indicate the regions over which model and aircraft are compared in Figure 10.

al., 2003]. Industrial regions are of particular interest here. The fossil fuel inventory is aseasonal in the a priori, however wintertime NO_x emissions in the a posteriori are larger than in the a priori by 50% near Beijing, and by 20–30% in the eastern United States. *Jaeglé et al.* [2005] and *Richter et al.* [2005] also found evidence of a wintertime maximum in Chinese NO_x emissions. Reductions in NO_x emissions from power plants are expected during May–September in the eastern United States with the largest changes along the Ohio River Valley [*Environmental Protection Agency*, 2003; *Frost et al.*, 2006].

[35] We reassess the effect of nonlinearity in equation (1) by incorporating the a posteriori inventory into the GEOS-Chem model, conducting a new simulation, and reapplying equations (1)–(3). The resultant top-down inventory increases by less than 5%, as expected from Figure 6. Small decreases in the resultant top-down inventory over major industrial areas are compensated by small increases elsewhere. As previously noted, a more nonlinear relationship may be expected in a higher resolution simulation.

[36] Sharp spatial gradients in NO_x chemistry also could affect the inference of emissions from SCIAMACHY NO_2 columns. We examine the potential sensitivity to model resolution by shifting the model grid by half of a grid box and repeating the analysis. The resultant a posteriori inventory decreases by 2%. Increases in NO_x emissions from some cities such as Los Angeles are compensated by decreases from others such as New York City.

[37] A recent manuscript [*van Noije et al.*, 2006] reveals that tropospheric NO_2 columns retrieved from GOME by the Dalhousie/SAO, BIRA/KNMI, and Bremen groups are generally consistent during summer but exhibit large systematic differences over industrial regions during wintertime. NO_2 columns retrieved by Dalhousie/SAO over industrial regions during wintertime tend to be systematically lower by 50% to 100% than those retrieved from the other groups. If those systematic biases exist between the different SCIAMACHY retrievals, NO_x emissions inferred from NO_2 columns retrieved by the BIRA/KNMI and Bremen groups over industrial regions during winter would be correspondingly larger than inferred here. Additional validation and intercomparison of SCIAMACHY retrievals is needed.

4.3. Evaluation of the A Posteriori Inventory

[38] We evaluate the a posteriori inventory by comparison with airborne in situ measurements, using the GEOS-Chem model as an intermediary. We focus on the region near New York City where the a priori and a posteriori inventories exhibited large differences and airborne measurements are available as part of ICARTT. Chemical ionization mass spectrometers on the WP-3D aircraft were used to measure PAN [*Flocke et al.*, 2005] and gas-phase HNO_3 [*Neuman et al.*, 2002].

[39] We include into the GEOS-Chem model the a posteriori inventory determined over May–October 2004, conduct a forward simulation, and examine the change in the simulation of reactive nitrogen. Figure 9 shows the resultant regional change in the GEOS-Chem simulation of NO_x, PAN, and HNO_3. The left panel shows that the largest change in NO_x occurs over the New York and Connecticut region where the largest change in emissions occurred. The middle panel shows a slightly more homogeneous increase in PAN of 100–200 pptv over most of New England. The right panel shows a more spatially uniform change in HNO_3, reflecting the longer HNO_3 lifetime of a few days in the lower troposphere. The simulated HNO_3 mixing ratio using the a posteriori inventory is 300–500 pptv larger over New England, Atlantic Canada, and into the North Atlantic Ocean.

[40] Figure 10 compares both the a priori and a posteriori inventories with in situ measurements taken as part of ICARTT. Both model and observations are averaged over the domains in which the a posteriori resulted in maximum differences in the model simulation as indicated by the white lines in Figure 9. In all three cases, the in situ measurements are more consistent with the a posteriori inventory than with the a priori. The mean model biases in the lower troposphere of NO_x and HNO_3 were reduced by 500 pptv, and by 200 pptv for PAN.

[41] We also evaluated the a posteriori inventory with in situ measurements from the DC-8 aircraft. Particular attention was given to the Ohio River Valley and New England.

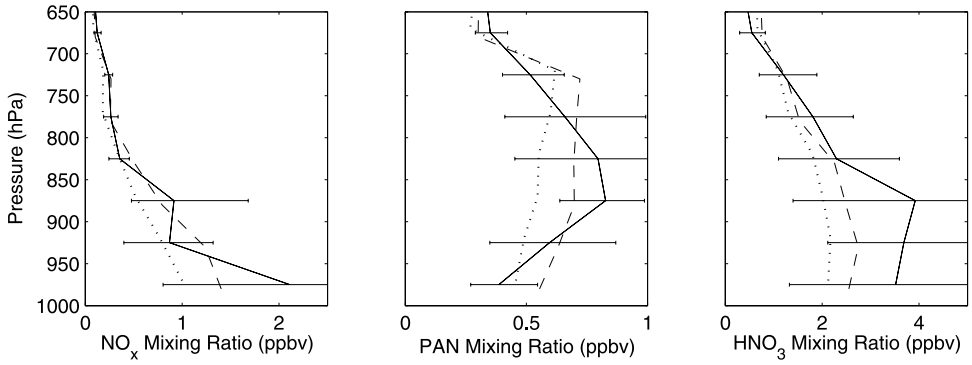

Figure 10. Mean vertical profiles of NO_x, PAN, and HNO_3 for the ensemble of WP-3D flights within the regions identified in Figure 9 over the period 5 July 2004 to 15 August 2004. Observations (solid lines, with 17th and 83rd percentiles as horizontal bars) are compared to model results sampled along the flight tracks at the measurement time using either the a priori NO_x inventory (dash-dotted lines) or the a posteriori NO_x inventory (dashed lines).

The comparison was inconclusive in all cases. Simulations of reactive nitrogen using either the a priori and a posteriori inventories exhibited little difference at the locations and times sampled by the DC-8 aircraft. Additional evaluation of the a posteriori inventory would be useful, especially downwind of China where pronounced differences exist versus the a priori.

5. Comparison of the A Posteriori With Previous Inventories

[42] We compare the a posteriori inventory with three commonly used bottom-up emission inventories and with previous inversions from GOME NO_2 columns. Figure 11 compares the a posteriori inventory with the EDGAR 3.2FT2000 inventory for 2000 [*Olivier et al.*, 2005]. The two inventories are moderately consistent (r^2 = 0.55, n = 3402). Part of the scatter arises from slight differences in the location of emissions in the two inventories in major industrial areas such as east China, northern Europe, and Houston. The global NO_x emission rate for the a posteriori inventory is 7% higher than that for EDGAR. A posteriori NO_x emissions tend to be higher than EDGAR emissions over industrial regions of the eastern United States, East Asia, and South Africa as well as numerous urban areas, but lower over Europe. The positive bias over the eastern United States in part reflects the influence of the outdated a priori on the a posteriori. Table 3 shows that regional totals in the a posteriori are generally more consistent with EDGAR than the a priori, likely reflecting more current information in EDGAR.

[43] Figure 12 compares the a posteriori inventory with the National Inventory for 1999 (NEI99) of the United States Environmental Protection Agency. The two inventories exhibit a high degree of consistency (r^2 = 0.82, n = 192). The a posteriori NO_x emission rate for the United States of 6.8 Tg N yr^{-1} is 0.2 Tg N yr^{-1} larger than that of NEI99. A posteriori NO_x emissions are about 25% lower than those for NEI99 over most of the eastern United States as expected from reductions in power plant emissions not included in NEI99 [*Environmental Protection Agency*, 2003; *Frost et al.*, 2006]. These decreases are compensated by higher NO_x emissions in the a posteriori than NEI99 for urban areas as may be associated with a hypothesized underestimate in mobile emissions [*Parrish et al.*, 2002], and for agricultural areas supporting earlier evidence of an underestimate in soil NO_x emissions [*Martin et al.*, 2003b; *Jaeglé et al.*, 2005].

[44] Figure 13 compares the a posteriori inventory with the bottom-up inventory of *Streets et al.* [2003] for eastern Asia for the year 2000. The spatial distribution of the two inventories is moderately consistent (r^2 = 0.64, n = 660). However, the regional magnitude of the a posteriori inventory of 14.3 Tg N yr^{-1} is 68% larger than that of *Streets et al.* [2003]. *Wang et al.* [2004] previously applied measurements of reactive nitrogen from the Transport and Chemical Evolution over the Pacific (TRACE-P) aircraft mission over

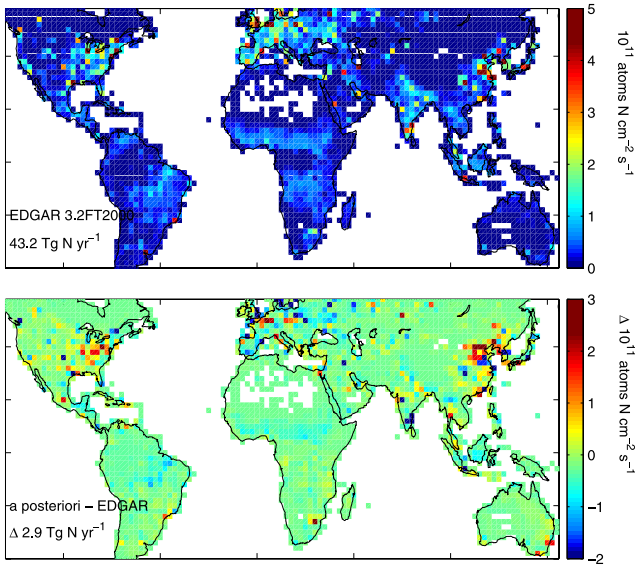

Figure 11. (top) Average surface NO_x emissions at 2° × 2.5° horizontal resolution from the EDGAR 3.2FT2000 inventory. The EDGAR inventory only includes industrial, biomass burning, and biofuel emissions. We add the GEOS-Chem soil NO_x emissions here for consistency. Annual global emissions are indicated in the bottom left. (bottom) Difference between the a posteriori and a priori inventories.

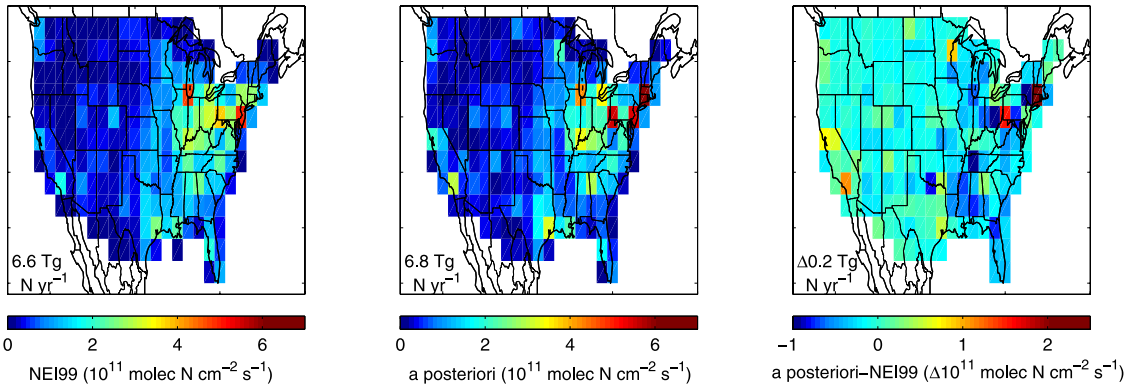

Figure 12. Annual average surface NO_x emissions at 2° × 2.5° horizontal resolution for the United States (left) from the National Emission Inventory for 1999 (NEI99) and (middle) from the a posteriori inventory. Annual regional totals are indicated in the bottom left. (right) Difference between the two inventories.

the northwest Pacific and from two ground stations during spring 2001 to constrain Asian NO_x emissions and found evidence for a 47% increase in Chinese NO_x emissions with respect to *Streets et al.* [2003]. The larger difference found here likely reflects recent growth in Asian NO_x emissions.

[45] Table 3 shows the regional totals in two a posteriori inventories determined from GOME NO_2 columns for 1996–1997 by *Martin et al.* [2003b], and for 2000 by *Jaeglé et al.* [2005]. The a posteriori inventory determined from SCIAMACHY is higher than that determined from GOME for most regions, likely reflecting recent global growth in NO_x emissions. Differences in the two measurements could also play a role in the higher SCIAMACHY inventory.

6. Conclusions

[46] We have constructed an improved inventory of current surface land NO_x emissions by combining top-down information from the SCIAMACHY satellite instrument with a priori information from a bottom-up inventory. Tropospheric NO_2 columns were retrieved from SCIAMACHY to provide the top-down constraint. The top-down constraint was determined over May 2004 to April 2005 to include the ICARTT campaign. Top-down emissions were determined through a simple inversion with a global chemical transport model (GEOS-Chem).

[47] We validated the tropospheric NO_2 columns with coincident in situ measurements from the NASA DC-8 and the NOAA WP-3D aircraft as part of the ICARTT campaign. Nearly 20 coincident measurements were found, providing an unprecedented validation opportunity over a wide range of conditions ranging from remote marine to highly polluted. The two measurements techniques were consistent within their uncertainty (r^2 = 0.60, geometric mean = 0.82, slope = 0.82). The SCIAMACHY columns tended to be lower than those determined from in situ measurements over polluted regions, and higher over remote regions, suggesting that NO_x emissions from megacities may be higher than reported here. As part of the validation, GEOS-Chem simulated vertical profiles of NO_2 used in the retrieval air mass factor calculation were compared with in situ measurements. A northern midlatitude lightning source of 1.6 Tg N yr^{-1} reduced the

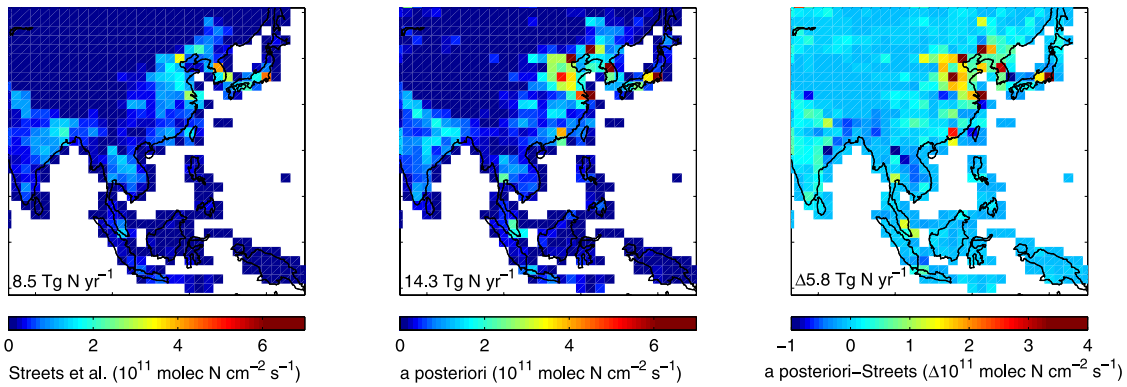

Figure 13. Annual average surface NO_x emissions at 2° × 2.5° horizontal resolution for eastern Asia from (left) the *Streets et al.* [2003] and (middle) the a posteriori inventory. The *Streets et al.* [2003] inventory only includes industrial and biofuel emissions. We add the GEOS-Chem soil and biomass burning NO_x emissions here for consistency. Annual regional totals are indicated in the bottom left. (right) Difference between the two inventories.

difference between airborne and simulated profiles; remaining differences would affect the retrieved NO_2 columns by a few percent.

[48] The increase in the simulated NO_2 columns from increased lightning NO_x emissions also reduced a model bias versus SCIAMACHY NO_2 columns over the North Atlantic Ocean where lightning makes a large relative contribution to the NO_2 column. SCIAMACHY NO_2 columns show a weak plume from North American lightning NO_x emissions that extends across the North Atlantic Ocean to Europe.

[49] Tropospheric NO_2 columns are highly heterogeneous over regions with isolated surface sources, providing empirical evidence of the short NO_x lifetime and high NO_2/NO_x ratio in the lower mixed layer that facilitate mapping of NO_x emissions from observed NO_2 columns over land. We evaluated the local relationship between NO_2 columns and land surface NO_x emissions by conducting sensitivity simulations over a range of emissions. We found a highly linear relationship at the resolution of $2^\circ \times 2.5^\circ$ used here; errors in the top-down estimate due to nonlinearity in the relationship about the a priori are less than 10% for a variety of locations.

[50] Our a posteriori inventory of 46.1 Tg N yr^{-1} is 22% higher than the GEIA-based a priori for 1998. Much of the increase is driven by emissions from East Asia. A posteriori NO_x emissions from East Asia (9.8 Tg N yr^{-1}) exceed those from North America or Europe. Comparison of the a posteriori and a priori inventory reveals significant underestimates in the a priori over several megacities outside of East Asia. The estimate of the global uncertainty in NO_x emissions is reduced from a factor of 2.3 in the a priori to a factor of 1.6 in the a posteriori.

[51] We evaluated the a posteriori inventory by including it in the GEOS-Chem model and comparing the resultant simulation over and downwind of New York City with in situ airborne measurements. The a posteriori inventory reduced the regional model bias in the lower troposphere of NO_x by 500 pptv, of PAN by 200 pptv, and of HNO_3 by 500 pptv, providing regional confidence in the a posteriori.

[52] We compared the a posteriori inventory with three other bottom-up inventories. The a posteriori inventory is 7% higher than that of the global EDGAR 3.2FT2000 for the year 2000, with pronounced differences over major industrial and urban areas. The a posteriori inventory of 6.8 Tg N yr^{-1} for the United States is 3% higher than the National Emission Inventory for 1999 of the Environmental Protection Agency. Higher NO_x emission rates in the urban centers and agricultural areas are offset by lower regional NO_x emission rates from much of the eastern United States. The a posteriori inventory for eastern Asia is 68% larger than that of *Streets et al.* [2003] for 2000 with most of the difference arising from major urban and industrial centers.

[53] Limitations in the current work that could introduce systematic errors in the a posteriori include possible biases in the cloud retrieval and surface reflectivity data set, zonal variability in the stratospheric NO_2 column, the outdated a priori, coarse model resolution, and horizontal smearing of the relationship between NO_2 columns and NO_x emissions. The development of a cloud retrieval that treats clouds as a collection of Mie scatterers rather than a Lambertian surface would enable a more accurate air mass factor calculation. A higher resolution surface reflectivity data set would better resolve spatial heterogeneity in urban areas. Representation of zonal variability in the stratospheric NO_2 column should improve the a posteriori inventory at high latitudes during winter. A more current a priori that accounts for recent trends in NO_x emissions would yield a more accurate a posteriori. Simulations at higher spatial resolution would better resolve the large spatial heterogeneity of urban areas apparent from SCIAMACHY observations, and better account for spatial variation in the NO_x lifetime in the inversion. An inverse analysis that quantitatively accounts for horizontal smearing should improve the accuracy of the inversion. Observations at higher resolution of 13 km by 24 km from the Ozone Monitoring Instrument onboard the Aura satellite soon will provide even greater detail and improve cloud screening.

[54] **Acknowledgments.** Three anonymous reviewers and Mark Lawrence provided constructive comments that improved the manuscript. We are grateful to the TEMIS project for making the FRESCO cloud fields publicly available. We thank the Netherlands SCIAMACHY Data Center (NL-SCIA-DC) for providing data and processing services. This work was supported by NASA's Radiation Science Program. The GEOS-Chem model is managed by the Atmospheric Chemistry Modeling Group at Harvard University with support from the NASA Atmospheric Chemistry Modeling and Analysis Program.

References

Adams, P. J., J. H. Seinfeld, D. Koch, L. Mickley, and D. Jacob (2001), General circulation model assessment of direct radiative forcing by the sulfate-nitrate-ammonium-water inorganic aerosol system, *J. Geophys. Res.*, *106*, 1097–1112.

Akimoto, H. (2003), Global air quality and pollution, *Science*, *302*, 1716–1719.

Alexander, B., J. Savarino, C. C. W. Lee, R. J. Park, D. J. Jacob, M. H. Thiemens, Q. B. Li, and R. M. Yantosca (2005), Sulfate formation in sea-salt aerosols: Constraints from oxygen isotopes, *J. Geophys. Res.*, *110*, D10307, doi:10.1029/2004JD005659.

Beirle, S., U. Platt, M. Wenig, and T. Wagner (2003), Weekly cycle of NO_2 by GOME measurements: A signature of anthropogenic sources, *Atmos. Chem. Phys.*, *3*, 2225–2232.

Beirle, S., U. Platt, M. Wenig, and T. Wagner (2004a), NO_x production by lightning estimated with GOME, *Adv. Space Res.*, *34*(4), 793–797.

Beirle, S., U. Platt, R. von Glasow, M. Wenig, and T. Wagner (2004b), Estimate of nitrogen oxide emissions from shipping by satellite remote sensing, *Geophys. Res. Lett.*, *31*, L18102, doi:10.1029/2004GL020312.

Beirle, S., et al. (2005), Estimating the NO_x produced by lightning from GOME and NLDN data: A case study in the Gulf of Mexico, *Am. Chem. Phys. Discuss.*, *5*, 11,295–11,329.

Benkovitz, C. M., M. T. Scholtz, J. Pacyna, L. Tarrason, J. Dignon, E. C. Voldner, P. A. Spiro, J. A. Logan, and T. E. Graedel (1996), Global gridded inventories for anthropogenic emissions of sulfur and nitrogen, *J. Geophys. Res.*, *101*, 29,239–29,253.

Berntsen, T. K., I. S. A. Isaksen, G. Myhre, S. Fuglestvedt, F. Stordal, T. Alsvik Larson, R. S. Freckleton, and K. P. Shine (1997), Effects of anthropogenic emissions on tropospheric ozone and its radiative forcing, *J. Geophys. Res.*, *102*, 28,101–28,126.

Bey, I., et al. (2001), Global modeling of tropospheric chemistry with assimilated meteorology: Model description and evaluation, *J. Geophys. Res.*, *106*, 23,073–23,096.

Boersma, K. F., H. J. Eskes, and E. J. Brinksma (2004), Error analysis for tropospheric NO_2 retrieval from space, *J. Geophys. Res.*, *109*, D04311, doi:10.1029/2003JD003962.

Boersma, K. F., H. J. Eskes, E. W. Meijer, and H. Kelder (2005), Estimates of lightning NO_x production from GOME satellite observations, *Am. Chem. Phys. Discuss.*, *5*, 3047–3104.

Bogumil, K., et al. (2003), Measurements of molecular absorption spectra with the SCIAMACHY pre-flight model: Instrument characterization and reference data for atmospheric remote-sensing in the 230–2380 nm region, *J. Photochem. Photobiol. A*, *157*, 167–184.

Bovensmann, H., J. P. Burrows, M. Buchwitz, J. Frerick, V. V. Rozanov, K. V. Chance, and A. P. H. Goede (1999), SCIAMACHY: Mission objectives and measurement modes, *J. Atmos. Sci.*, *56*, 127–150.

Brasseur, G. P., J. T. Kiehl, J.-F. Muller, T. Schneider, C. Granier, X. X. Tie, and D. Hauglustaine (1998), Past and future changes in global tropospheric ozone: Impact on radiative forcing, *Geophys. Res. Lett.*, *25*, 3807–3810.

Burrows, J. P., et al. (1999), The Global Ozone Monitoring Experiment (GOME): Mission concept and first scientific results, *J. Atmos. Sci.*, *56*, 151–175.

Chance, K. (1998), Analysis of BrO measurements from the Global Ozone Monitoring Experiment, *Geophys. Res. Lett.*, *25*, 3335–3338.

Chance, K. V., and R. J. D. Spurr (1997), Ring effect studies: Rayleigh scattering, including molecular parameters for rotational Raman scattering, and the Fraunhofer spectrum, *Appl. Opt.*, *36*, 5224–5230.

Choi, Y., Y. Wang, T. Zeng, R. V. Martin, T. P. Kurosu, and K. Chance (2005), Evidence of lightning NO_x and convective transport of pollutants in satellite observations over North America, *Geophys. Res. Lett.*, *32*, L02805, doi:10.1029/2004GL021436.

Christian, H. J., et al. (2003), Global frequency and distribution of lightning as observed from space by the Optical Transient Detector, *J. Geophys. Res.*, *108*(D1), 4005, doi:10.1029/2002JD002347.

DeCaria, A. J., K. E. Pickering, G. L. Stenchikov, and L. E. Ott (2005), Lightning-generated NO_x and its impact on tropospheric ozone production: A three-dimensional modeling study of a Stratosphere-Troposphere Experiment: Radiation, Aerosols and Ozone (STERAO-A) thunderstorm, *J. Geophys. Res.*, *110*, D14303, doi:10.1029/2004JD005556.

Derwent, R. G., D. S. Stevenson, W. J. Collins, and C. E. Johnson (2004), Intercontinental transport and the origins of the ozone observed at surface sites in Europe, *Atmos. Environ.*, *38*, 1891–1901.

Duncan, B. N., R. V. Martin, A. C. Staudt, R. M. Yevich, and J. A. Logan (2003), Interannual and seasonal variability of biomass burning emissions constrained by remote-sensed observations, *J. Geophys. Res.*, *108*(D2), 4100, doi:10.1029/2002JD002378.

Edwards, D. P., et al. (2003), Tropospheric ozone over the tropical Atlantic: A satellite perspective, *J. Geophys. Res.*, *108*(D9), 4237, doi:10.1029/2002JD002927.

Environmental Protection Agency (1989), The 1985 NAPAP emission inventory (version 2): Development of the annual data and modeler's tapes, *EPA-600/7-89-012a*, Research Triangle Park, N. C.

Environmental Protection Agency (2003), National air quality and emissions trends report: 2003 special studies edition, report, 190 pp., Research Triangle Park, N. C.

European Space Agency (1995), *The GOME Users Manual*, edited by F. Bednarz, ESA Publ. Div., Eur. Space Res. and Tech. Cent., Noordwijk, Netherlands.

Evans, M. J., and D. J. Jacob (2005), Impact of new laboratory studies of N_2O_5 hydrolysis on global model budgets of tropospheric nitrogen oxides, ozone, and OH, *Geophys. Res. Lett.*, *32*, L09813, doi:10.1029/2005GL022469.

Fehr, T., H. Holler, and H. Huntrieser (2004), Model study on production and transport of lightning-produced NOx in a EULINOX supercell storm, *J. Geophys. Res.*, *109*, D09102, doi:10.1029/2003JD003935.

Fiore, A. M., D. J. Jacob, I. Bey, R. M. Yantosca, B. D. Field, and J. G. Wilkinson (2002), Background ozone over the United States in summer: Origin and contribution to pollution episodes, *J. Geophys. Res.*, *107*(D15), 4275, doi:10.1029/2001JD000982.

Flocke, F. M., A. Swanson, A. W. Weinheimer, J. M. Roberts, R. Schmitt, and S. Shertz (2005), On the measurement of PANs by gas chromatography and electron capture detection, *J. Atmos. Chem.*, *52*, 19–43.

Frost, G. J., et al. (2006), Effects of changing power plant NO_x emissions on ozone in the eastern United States: Proof of concept, *J. Geophys. Res.*, *111*, D12306, doi:10.1029/2005JD006354.

Greenblatt, G. D., J. J. Orlando, J. B. Burkholder, and A. R. Ravishankara (1990), Absorption measurements of oxygen between 330 and 1140 nm, *J. Geophys. Res.*, *95*, 18,577–18,585.

He, K. B., H. Huo, Q. Zhang, D. Q. He, F. An, M. Wang, and M. P. Walsh (2005), Oil consumption and CO_2 emissions in China's road transport: Current status, future trends, and policy implications, *Energy Policy*, *33*, 1499–1507.

Heue, K.-P., et al. (2005), Validation of SCIAMACHY tropospheric NO_2-columns with AMAXDOAS measurements, *Atmos. Chem. Phys.*, *5*, 1039–1051.

Hirsch, R. M., and E. J. Gilroy (1984), Methods of fitting a straight line to data: Examples in water resources, *Water Resour. Bull.*, *20*, 705–711.

Holland, E. A., and J.-F. Lamarque (1997), Modeling bio-atmospheric coupling of the nitrogen cycle through NO_x emissions and NO_y deposition, *Nutr. Cycl. Agroecosyst.*, *48*, 7–24.

Intergovernmental Panel on Climate Change (2001), *Climate Change 2001: The Scientific Basis*, 881 pp., Cambridge Univ. Press, New York.

Jacob, D. J. (2000), Heterogeneous chemistry and tropospheric ozone, *Atmos. Environ.*, *34*, 2131–2159.

Jacob, D. J., et al. (1993), Simulation of summertime ozone over North America, *J. Geophys. Res.*, *98*, 14,797–14,816.

Jacob, D. J., et al. (1996), Origin of ozone and NO_x in the tropical troposphere: A photochemical analysis of aircraft observations over the South Atlantic basin, *J. Geophys. Res.*, *101*, 24,235–24,250.

Jacob, D. J., J. A. Logan, and P. P. Murti (1999), Effect of rising Asian emissions on surface ozone in the United States, *Geophys. Res. Lett.*, *26*, 2175–2178.

Jaeglé, L., et al. (2004), Satellite mapping of rain-induced nitric oxide emissions from soils, *J. Geophys. Res.*, *109*, D21310, doi:10.1029/2004JD004787.

Jaeglé, L., L. Steinberger, R. V. Martin, and K. Chance (2005), Global partitioning of NO_x sources using satellite observations: Relative roles of fossil fuel combustion, biomass burning and soil emissions, *Faraday Discuss.*, *130*, 407–423, doi:10.1039/b502128f.

Kasibhatla, P. S., H. Levy, W. J. Moxim, and W. L. Chameides (1991), The relative importance of stratospheric photochemical production on tropospheric NO_y levels: A model study, *J. Geophys. Res.*, *96*, 18,631–18,646.

Koelemeijer, R. B. A., P. Stammes, J. W. Hovenier, and J. F. de Haan (2002), Global distributions of effective cloud fraction and cloud top pressure derived from oxygen A band spectra measured by the Global Ozone Monitoring Experiment: Comparison to ISCCP data, *J. Geophys. Res.*, *107*(D12), 4151, doi:10.1029/2001JD000840.

Koelemeijer, R. B. A., J. F. de Haan, and P. Stammes (2003), A database of spectral surface reflectivity of the Earth in the range 335–772 nm derived from 5.5 years of GOME observations, *J. Geophys. Res.*, *108*(D2), 4070, doi:10.1029/2002JD002429.

Kunhikrishnan, T., and M. G. Lawrence (2004), Sensitivity of NO_x over the Indian Ocean to emissions from the surrounding continents and nonlinearities in atmospheric chemistry responses, *Geophys. Res. Lett.*, *31*, L15109, doi:10.1029/2004GL020210.

Lelieveld, J., et al. (2002), Global air pollution crossroads over the Mediterranean, *Science*, *298*, 794–799.

Leue, C., M. Wenig, T. Wagner, O. Klimm, U. Platt, and B. Jahne (2001), Quantitative analysis of NO_x emissions from GOME satellite image sequences, *J. Geophys. Res.*, *106*, 5493–5505.

Li, Q. B., D. J. Jacob, R. M. Yantosca, J. W. Munger, and D. D. Parrish (2004), Export of NO_y from the North American boundary layer: Reconciling aircraft observations and global model budgets, *J. Geophys. Res.*, *109*, D02313, doi:10.1029/2003JD004086.

Martin, R. V., et al. (2002a), Interpretation of TOMS observations of tropical tropospheric ozone with a global model and in-situ observations, *J. Geophys. Res.*, *107*(D18), 4351, doi:10.1029/2001JD001480.

Martin, R. V., et al. (2002b), An improved retrieval of tropospheric nitrogen dioxide from GOME, *J. Geophys. Res.*, *107*(D20), 4437, doi:10.1029/2001JD001027.

Martin, R. V., D. J. Jacob, R. M. Yantosca, M. Chin, and P. Ginoux (2003a), Global and regional decreases in tropospheric oxidants from photochemical effects of aerosols, *J. Geophys. Res.*, *108*(D3), 4097, doi:10.1029/2002JD002622.

Martin, R. V., D. J. Jacob, K. Chance, T. P. Kurosu, P. I. Palmer, and M. J. Evans (2003b), Global inventory of nitrogen oxide emissions constrained by space-based observations of NO_2 columns, *J. Geophys. Res.*, *108*(D17), 4537, doi:10.1029/2003JD003453.

Martin, R. V., et al. (2004), Evaluation of GOME satellite measurements of tropospheric NO_2 and HCHO using regional data from aircraft campaigns in the southeastern United States, *J. Geophys. Res.*, *109*, D24307, doi:10.1029/2004JD004869.

Michaels, A. F., D. Olson, J. L. Sarmiento, J. W. Ammerman, K. Fanning, R. Jahnke, A. H. Knap, F. Lipschultz, and J. M. Prospero (1996), Inputs, losses and transformations of nitrogen and phosphorus in the pelagic North Atlantic Ocean, *Biogeochemistry*, *35*, 181–226.

Müller, J.-F., and T. Stavrakou (2005), Inversion of CO and NO_x emissions using the adjoint of the IMAGES model, *Am. Chem. Phys.*, *5*, 1157–1186.

Murphy, D., D. Fahey, M. Proffitt, S. Liu, C. Eubank, S. Kawa, and K. Kelly (1993), Reactive odd nitrogen and its correlation with ozone in the lower stratosphere and upper troposphere, *J. Geophys. Res.*, *98*, 8751–8773.

Nenes, A., R. J. Charlson, M. C. Facchini, M. Kulmala, A. Laaksonen, and J. H. Seinfeld (2002), Can chemical effects on cloud droplet number rival the first indirect effect?, *Geophys. Res. Lett.*, *29*(17), 1848, doi:10.1029/2002GL015295.

Neuman, J. A., et al. (2002), Fast-response airborne in situ measurements of HNO 3 during the Texas 2000 Air Quality Study, *J. Geophys. Res.*, *107*(D20), 4436, doi:10.1029/2001JD001437.

Olivier, J. G. J., J. A. Van Aardenne, F. Dentener, L. Ganzeveld, and J. A. H. W. Peters (2005), Recent trends in global greenhouse gas emissions: Regional trends and spatial distribution of key sources, in *Non-CO_2*

Greenhouse Gases (NCGG-4), edited by A. V. Amstel, pp. 325–330, Millpress, Rotterdam, Netherlands.

Palmer, P. I., et al. (2001), Air mass factor formulation for spectroscopic measurements from satellites: Application to formaldehyde retrievals from the Global Ozone Monitoring Experiment, *J. Geophys. Res.*, *106*, 14,539–14,550.

Palmer, P. I., D. J. Jacob, A. M. Fiore, R. V. Martin, K. Chance, and T. P. Kurosu (2003), Mapping isoprene emissions over North America using formaldehyde column observations from space, *J. Geophys. Res.*, *108*(D6), 4180, doi:10.1029/2002JD002153.

Park, R. J., D. J. Jacob, M. Chin, and R. V. Martin (2003), Sources of carbonaceous aerosols over the United States and implications for natural visibility conditions, *J. Geophys. Res.*, *108*(D12), 4355, doi:10.1029/2002JD003190.

Park, R. J., D. J. Jacob, B. D. Field, R. M. Yantosca, and M. Chin (2004), Natural and transboundary pollution influences on sulfate-nitrate-ammonium aerosols in the United States: Implications for policy, *J. Geophys. Res.*, *109*, D15204, doi:10.1029/2003JD004473.

Park, R. J., et al. (2005), Export efficiency of black carbon aerosol in continental outflow: Global implications, *J. Geophys. Res.*, *110*, D11205, doi:10.1029/2004JD005432.

Parrish, D. D., M. Trainer, D. Hereld, E. J. Williams, K. J. Olszyna, R. A. Harley, J. F. Meagher, and F. C. Fehsenfeld (2002), Decadal change in carbon monoxide to nitrogen oxide ratio in the U.S. vehicular emissions, *J. Geophys. Res.*, *107*(D12), 4140, doi:10.1029/2001JD000720.

Penner, J. E., C. S. Athertson, J. Dignon, S. J. Ghan, J. J. Walton, and S. Hameed (1991), Tropospheric nitrogen: A three-dimensional study of sources, distributions, and deposition, *J. Geophys. Res.*, *96*, 959–990.

Pickering, K. E., Y. S. Wang, W. K. Tao, C. Price, and J. F. Muller (1998), Vertical distributions of lightning NO_x for use in regional and global chemical transport models, *J. Geophys. Res.*, *103*, 31,203–31,216.

Prather, M. J., et al. (2001), Atmospheric chemistry and greenhouse gases, in *Climate Change 2001: The Scientific Basis*, edited by J. T. Houghton et al., pp. 239–287, Cambridge Univ. Press, New York.

Price, C., and D. Rind (1992), A simple lightning parameterization for calculating global lightning distributions, *J. Geophys. Res.*, *97*, 9919–9933.

Price, C., J. Penner, and M. Prather (1997), NO_x from lightning: 1. Global distribution based on lightning physics, *J. Geophys. Res.*, *102*, 5929–5941.

Richter, A., and J. P. Burrows (2002), Tropospheric NO_2 from GOME measurements, *Adv. Space Res.*, *29*, 1673–1683.

Richter, A., and T. Wagner (2001), Diffuser plate spectral structures and their influence on GOME slant columns, technical note, 4 pp., Univ. of Bremen, Bremen, Germany.

Richter, A., V. Eyring, J. P. Burrows, H. Bovensmann, A. Lauer, B. Sierk, and P. J. Crutzen (2004), Satellite measurements of NO_2 from international shipping emissions, *Geophys. Res. Lett.*, *31*, L23110, doi:10.1029/2004GL020822.

Richter, A., J. P. Burrows, H. Nüß, C. Granier, and U. Niemeier (2005), Significant increase in tropospheric nitrogen dioxide over China observed from space, *Nature*, *437*, 129–132, doi:10.1038/nature04092.

Rothman, L. S., et al. (1998), The HITRAN molecular spectroscopic database and HAWKS (HITRAN atmospheric workstation): 1996 edition, *J. Quant. Spectrosc. Radiat. Transfer*, *60*, 665–710.

Ryerson, T. B., et al. (2003), Effect of petrochemical industrial emissions of reactive alkenes and NO_x on tropospheric ozone formation in Houston, Texas, *J. Geophys. Res.*, *108*(D8), 4249, doi:10.1029/2002JD003070.

Spurr, R. J. D. (2002), Simultaneous derivation of intensities and weighting functions in a general pseudo-spherical discrete ordinate radiative transfer treatment, *J. Quant. Spectrosc. Radiat. Transfer*, *75*, 129–175.

Spurr, R. J. D., T. P. Kurosu, and K. V. Chance (2001), A linearized discrete ordinate radiative transfer model for atmospheric remote sensing retrieval, *J. Quant. Spectrosc. Radiat. Transfer*, *68*, 689–735.

Streets, D., et al. (2003), An inventory of gaseous and primary aerosol emissions in Asia in the year 2000, *J. Geophys. Res.*, *108*(D21), 8809, doi:10.1029/2002JD003093.

Thornton, J. A., P. J. Wooldridge, and R. C. Cohen (2000), Atmospheric NO_2: In situ laser-induced fluorescence detection at parts per trillion mixing ratios, *Anal. Chem.*, *72*, 528–539.

van Noije, T. P. C., et al. (2006), Multi-model ensemble simulations of tropospheric NO_2 compared with GOME retrievals for the year 2000, *Am. Chem. Phys. Discuss.*, *6*, 2965–3047.

Wang, Y., D. J. Jacob, and J. A. Logan (1998), Global simulation of tropospheric O_3 - NO_x - hydrocarbon chemistry: 1. Model formulation, *J. Geophys. Res.*, *103*, 10,713–10,726.

Wang, Y. X., M. B. McElroy, T. Wang, and P. I. Palmer (2004), Asian emissions of CO and NO_x: Constraints from aircraft and Chinese station data, *J. Geophys. Res.*, *109*, D24304, doi:10.1029/2004JD005250.

Wild, O., M. J. Prather, and H. Akimoto (2001), Indirect long-term global cooling from NO_x emissions, *Geophys. Res. Lett.*, *28*, 1719–1722.

Yienger, J. J., and H. Levy (1995), Empirical model of global soil-biogenic NO_x emissions, *J. Geophys. Res.*, *100*, 11,447–11,464.

T. H. Bertram, R. C. Cohen, and P. J. Wooldridge, Department of Chemistry, University of California, Berkeley, Berkeley, CA 94720-1640, USA. (tbertram@berkeley.edu; cohen@cchem.berkeley.edu; pjwool@socrates.berkeley.edu)

K. Chance and C. E. Sioris, Harvard-Smithsonian Center for Astrophysics, Cambridge, MA 02138-1516, USA. (kchance@cfa.harvard.edu; csioris@cfa.harvard.edu)

F. M. Flocke, Atmospheric Chemistry Division, National Center for Atmospheric Research, Boulder, CO 80307, USA. (ffl@ucar.edu)

R. V. Martin, Department of Physics and Atmospheric Science, Dalhousie University, Halifax, NS B3H 3J5, Canada. (randall.martin@dal.ca)

J. A. Neuman, T. B. Ryerson, and A. Swanson, Chemical Sciences Division, Earth System Research Laboratory, NOAA, Boulder, CO 80307, USA. (andy.neuman@noaa.gov; thomas.b.ryerson@noaa.gov)